Deutsches Elektronen-Synchrotron (DESY)
Hamburg

Report for the 2019 Summer Student Program

on

Higgs CP Characterization using Higgs Production in Association with a Z Boson

Lisa Biermann, Karlsruhe Institute of Technology (KIT), Germany

supervised by

Prof. Dr. Georg Weiglein

Dr. Tim Stefaniak and Dr. Henning Bahl

Dr. Matthias Saimpert

Abstract

We study the CP nature of the Higgs top Yukawa coupling by Z boson associated Higgs production of a non-Standard Model Higgs-top interaction using the framework of the Higgs Characterization Model. The 125 GeV Higgs boson is modelled as a CP mixed state, parametrized by an angle α. The event generation is done via MadGraph5_aMC@NLO, Pythia 8 and Delphes 3. The event selection follows the measurement of $pp \to ZH$ production with a $b\bar{b}$ final state done by the ATLAS collaboration. The gluon induced Z boson associated Higgs production process is found to be sensitive to a change of the CP mixing angle α. The cross section increases and p_T distributions show a harder spectrum for higher α. The quark induced Z boson associated Higgs production process is found to be not sensitive to a change in the CP mixing angle α. The signal yield and signal strength are predicted to increase with higher α.

September 2019

Contents

1 Introduction

With the discovery of a Higgs boson in 2012 by ATLAS and CMS [1, 2], one candidate for the last missing particle in the Standard Model (SM) of particle physics was found. Strong efforts were and are made to test the properties of the found particle. Assuming that the observed resonance can be explained by one new particle, experiments do favour the SM hypothesis of a scalar particle. ATLAS and CMS do exclude the hypothesis of $s^{CP} = 0^-$ at the 3σ confidence level looking at the $H \to \gamma\gamma$, $H \to ZZ^* \to 4l$, $H \to WW^* \to l\nu l\nu$ and $H \to ZZ$ channels [3, 4].

The goal of this work is to study the consequences and physical implications of a CP-violating $Ht\bar{t}$ coupling which is not yet constrained by experiments. Therefore, the process of Z boson associated production is chosen because it is sensitive to a CP odd component of the $Ht\bar{t}$ coupling. For modelling of a BSM $Ht\bar{t}$ coupling, a general approach with an Effective Field Theory (EFT) is used. The additional BSM physics is described taking into account the operator with the lowest possible energy dimension which modifies the Higgs-top Yukawa interaction. It is formulated such that the CP mixing is parametrized by a mixing angle α which allows for a clear visualization of the mixing angle dependence of collider observables.

After an introduction to the process of Z boson associated Higgs production in section 2.1, the formalism of an EFT is further explained in section 2.2. The computational framework used is introduced in section 3. The main components used for event generation are the matrix element generator MadGraph5_aMC@NLO [5], the shower and hadronization simulation tool Pythia 8 [6] and Delphes 3 [7] which is a detector simulation program. The process of event selection is described in section 3.2.

Another goal of this work is the comparison of the predictions made for a BSM $Ht\bar{t}$ coupling with an experimental analysis which is sensitive to the studied process. The results from the ATLAS search for Z boson associated Higgs production with $H \to b\bar{b}$ [8] are used for comparison and discussion in section 4. Section 4.1 presents the calculated cross sections, section 4.2 compares distributions of different observables and section 4.3 and 4.4 discusses signal yields and signal strengths. The work is summarized in section 5.

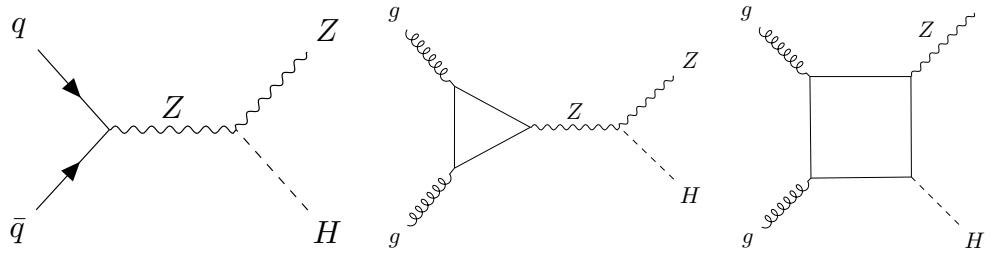

(a) quark initial state

(b) gluon initial state with triangle quark loop and s-channel Z-exchange

(c) gluon initial state box diagram

Figure 1: Processes contributing to LO Z boson associated H production

2 Theoretical Framework

We study the effect of a BSM Higgs CP character on the process of Z boson associated Higgs production. The process is discussed in section 2.1. Section 2.2 introduces the Higgs Characterization (HC) Model, i.e. a theoretical framework describing BSM effects in an EFT approach.

2.1 Z Boson Associated Higgs Production in Proton-Proton Collisions

At leading order (LO) there are three diagrams contributing to pp fusion with Z boson associated Higgs production. Either a quark and an antiquark of the same flavour can annihilate producing a Z boson which then radiates off a Higgs boson H, see figure 1a, or two gluons participate in a loop-induced process producing the Z and H boson, see figure 1b and 1c. In the latter process, the Higgs can either be radiated off of the Z boson (1b), or it is produced from the internal quark line within the box diagram (1c). This process is therefore sensitive to a BSM coupling of the measured boson H to t quarks. The effect of a CP-admixture on this process will be further studied in this work.

2.2 The Higgs Characterization Model

An effective field theory (EFT) offers a universal approach to study a general boson with spin s and CP character which ought to explain the experimental observation. The SM Lagrangian does already contain all Lorentz and gauge invariant permutations of fields with mass dimension four. To include effects of new physics the SM Lagrangian without the Higgs term $\mathcal{L}_{\text{SM-H}}$ gets expanded by adding higher dimension operators consisting of SM fields and respecting gauge and Lorentz symmetry.

$$\mathcal{L}_{\text{EFT}} = \mathcal{L}_{\text{SM-H}} + \sum_{d>4} \sum_{i=1}^{N} \frac{f_i^{(d)}}{\Lambda^{(d-4)}} \mathcal{O}_i^{(d)} \tag{1}$$

The additional terms have to be divided by Λ^{d-4} with energy dimension d to have an overall energy dimension of 4 which ensures a dimensionless action. Λ defines the limited validity range of an EFT. Only if all possible operators could be considered, an EFT restores unitarity. If only a finite number of additional terms are included, an EFT violates unitarity for energies above the limited validity

range. Assuming that the experimentally observed resonance can be explained by one new bosonic state $X(s^{CP})$, the effective Lagrangian is written as

$$\mathcal{L}_{HC} = \mathcal{L}_{\text{SM-H}} + \mathcal{L}_{X(s^{CP})}. \tag{2}$$

The spin of the new bosonic state is set in the following to the experimentally favoured $s = 0$ and the new boson will be referred to as X_0, observing just the effect of different CP characters on the observable parameters. Additionally, only modifications to the coupling of the new boson to the t quarks are considered. If the interactions with t quarks can be dominantly described by operators with the lowest possible energy dimension, then only one dimension six operator is modifying the Yukawa interaction. The corresponding Lagrangian is

$$\mathcal{L}_Y^{(6)} = \frac{f_Y^{(6)}}{\Lambda^2}\left(\Phi^\dagger\Phi\right)\overline{Q}_L\widetilde{\Phi}\,t_R + h.c., \tag{3}$$

with the Higgs doublet field Φ and the SU(2)-doublet of the third generation quarks $Q_L = (t_L, b_L) = P_L(t, b) = P_L Q$. Using $\gamma_5^\dagger = \gamma_5$, $P_{L/R} = \frac{1\mp\gamma_5}{2}$ and $\{\gamma_5, \gamma_0\} = 0$ leads to

$$\overline{Q_L} = Q_L^\dagger\gamma_0 = (P_L Q)^\dagger\gamma_0 = Q^\dagger P_L\gamma_0 = Q^\dagger\gamma_0 P_R = \overline{Q}P_R. \tag{4}$$

Inserting equation (4) and

$$\widetilde{\Phi} = i\sigma_2\Phi^* = i\sigma_2\begin{pmatrix}\phi^\mp \\ \frac{1}{\sqrt{2}}(v + H - i\phi_0)\end{pmatrix} = \begin{pmatrix}\frac{1}{\sqrt{2}}(v + H - i\phi_0) \\ -\phi^\mp\end{pmatrix} \tag{5}$$

into equation (3) and only taking the terms modifiying the $Ht\bar{t}$ coupling into account, leads to

$$\begin{aligned}\mathcal{L}_{Y,Ht\bar{t}}^{(6)} &= \frac{3}{2\sqrt{2}}\frac{f_Y^{(6)}}{\Lambda^2}v^2\bar{t}HP_R t + h.c. &(6)\\ &= \frac{3}{2\sqrt{2}}\frac{v^2}{\Lambda^2}\left(f_Y^{(6)}H\bar{t}P_R t + f_Y^{(6)*}H\bar{t}P_L t\right) \\ &= \frac{3}{2\sqrt{2}}\frac{v^2}{\Lambda^2}\left(\left(f_Y^{(6)} + f_Y^{(6)*}\right)H\bar{t}t + \left(f_Y^{(6)} - f_Y^{(6)*}\right)H\bar{t}\gamma_5 t\right) \\ &= \frac{3}{2\sqrt{2}}\frac{v^2}{\Lambda^2}\left(2\,\text{Re}\left(f_Y^{(6)}\right)H\bar{t}t + 2i\,\text{Im}\left(f_Y^{(6)}\right)H\bar{t}\gamma_5 t\right). &(7)\end{aligned}$$

In the Higgs Characterization (HC) model [9] the Higgs fermion interaction is a generalization of the Higgs Yukawa coupling and described by the parametrization

$$\frac{3}{\sqrt{2}}\,\text{Re}\left(f_Y^{(6)}\right) = \frac{\Lambda^2}{v^2}\left(c_\alpha\kappa_{Htt}g_{Htt} - g_{Htt}\right) \tag{8}$$

$$\frac{3}{\sqrt{2}}i\,\text{Im}\left(f_Y^{(6)}\right) = \frac{\Lambda^2}{v^2}i\left(s_\alpha\kappa_{att}g_{att}\right) \tag{9}$$

with $c_\alpha = \cos(\alpha)$ and $s_\alpha = \sin(\alpha)$. $\text{Re}\left(f_Y^{(6)}\right)$ is chosen such that the SM Higgs-top Yukawa coupling term gets compensated. This results in

$$\mathcal{L}_{HC}^t = -\bar{t}\left(c_\alpha\kappa_{Htt}g_{Htt} + is_\alpha\kappa_{att}g_{att}\gamma_5\right)tX_0. \tag{10}$$

This framework only has two free parameters, but it is chosen to have the additional parameter α which is an angle describing the mixing between CP even (0^+) and CP odd (0^-) character of X_0.

Table 1: Choice of parameters in HC model

	c_α	κ_{SM}	κ_{Htt}	κ_{Att}
$\alpha = 0°$	1	1	1	0
$\alpha = 18°$	0.9487	1.0541	1	1
$\alpha = 45°$	$1/\sqrt{2}$	$\sqrt{2}$	1	1
$\alpha = 72°$	0.3162	3.1623	1	1
$\alpha = 90°$	$1/\sqrt{2}$	$\sqrt{2}$	0	$\sqrt{2}$
$\alpha = 135°$	$-1/\sqrt{2}$	$-\sqrt{2}$	1	1
$\alpha = 180°$	-1	-1	1	0

Table 2: Behaviour of scalars and pseudoscalars under charge and parity transformation [10]

	$\bar{\Psi}\Psi$	$i\bar{\Psi}\gamma_5\Psi$
$\mathcal{P}$	1	-1
$\mathcal{C}$	1	1

g_{hff} names the scalar, g_{aff} names the pseudoscalar coupling strength, $g_{aff} = g_{Htt} = \frac{m_t}{v}$. κ_{Htt} and κ_{att} are additional dimensionless coupling parameters. As additional boundary conditions

$$\left|c_\alpha^2\kappa_{Htt}^2 + s_\alpha^2\kappa_{att}^2\right| \sim 1 \quad \text{and} \quad c_\alpha\kappa_{\mathrm{SM}} \sim 1 \tag{11}$$

are chosen. κ_{SM} is the dimensionless coupling parameter of the SM. The SM Higgs Yukawa coupling to top quarks is reproduced by setting $\alpha = 0$, $\kappa_{SM} = 1$, $\kappa_{Htt} = 1$ and $\kappa_{att} = 0$. Then

$$\mathcal{L}^t_{0,\,\text{pure CP even}} = -g_{Htt}\bar{t}tX_0 \tag{12}$$

which transforms as a scalar under CP transformation. For a pure CP odd X_0 boson ($\alpha = 90°$) with parameters chosen as displayed in table 1 the Lagrangian reads

$$\mathcal{L}^t_{0,\,\text{pure CP odd}} = -ig_{att}\bar{t}\gamma_5 tX_0 \tag{13}$$

and transforms like a pseudoscalar under CP transformation. The transformation of a scalar and a pseudoscalar under parity transformation $\mathcal{P}$ and charge conjugation $\mathcal{C}$ can be found in table 2.

In this work we examine a CP mixed boson whose mixing between CP even and odd is parametrized via α. For a CP mixed boson the dimensionless coupling parameters are set to $\kappa_{Htt} = \kappa_{att} = 1$. For comparison seven different values of α are used, the chosen parameters for each case can be found in table 1. Inserting values of the other parameters, the state of $\alpha = 45°$ corresponds to 50 % of CP odd and 50 % CP even character of the boson $s_\alpha/c_\alpha = 1$ leading to the Lagrangian

$$\mathcal{L}^t_{0,\,\alpha=45°} = \frac{1}{\sqrt{2}}\bar{t}\left(g_{Htt} - ig_{att}\gamma_5\right)tX_0. \tag{14}$$

Additionally, the cases $s_\alpha/c_\alpha = 1/3$ and $s_\alpha/c_\alpha = 3$ are considered which correspond to 75 % CP even and 25 % CP odd and 25 % CP even and 75 % CP odd respectively. The cases with $\alpha = 135°$ and $\alpha = 180°$ correspond to a negative c_α and κ_{SM}.

3 Computational Framework

Doing precision calculations for processes happening at pp colliders requires powerful tools able to simulate effects of Quantum Chromodynamics (QCD) which describes the interactions between partons. A Monte Carlo (MC) event generator enables the simulation of the final state particles and their angular and momentum distribution for particle collisions. The framework of the event generation using MadGraph5_aMC@NLO [5] is explained in section 3.1. Section 3.2 does describe the workflow of imposing experimentally motivated cuts on the data following the event selection of the $pp \to ZH$, $H \to b\bar{b}$ analysis presented by the ATLAS collaboration [8].

3.1 Event Generation

The inner structure of the proton is described by the parton model [11]. Parton Distribution Functions (PDFs) which are provided by LHAPDF [12] describe the momenta and flavour of the incoming proton constituents, namely quarks and gluons.

The factorization theorem [13] allows the separation of the hard process, which is calculable in a perturbative framework, from the soft process. The computational framework of this work uses the methods of MadGraph5_aMC@NLO [5] as the generator of the matrix element for the hard scattering process. As an input it takes a process and a model file which includes all Feynman rules calculated from the considered model Lagrangian. The Mathematica [14] package FeynRules [15] provides the model in an Universal Feynrules Output (UFO) file. Given the process, the matrix element is calculated including all possible Feynman diagrams up to loop level for the processes with a $q\bar{q}$ and gg initial state which are displayed for LO in figure 1a-1c.

The generation of one loop matrix elements is done via MadLoop [16]. The hard scattering process does also include the leptonic decay of $Z \to l^+l^-$ with $l = e, \mu$ and the decay of X_0 into $X_0 \to b\bar{b}$ which is implemented using MadEvent [17, 18]. MadSpin [19] offers an efficient and automatic mechanism to keep track of spin correlations.

Some code snippets neccesary to generate events using the MadGraph5_aMC@NLO interface are displayed in the following.

At first the Higgs Characterization Model in UFO format provided by [20] is loaded.

```
> import model HC_NLO_X0
```

The generation of the process $gg \to ZH$ is done by implementing the leptonic decay of the Z boson. `l+` and `l-` are including muons and electrons, the option `/ a` excludes the production of a X_0 boson associated with a photon γ and `[QCD]` enables the loop-induced mode.

```
> generate g g > x0 l+ l- / a [QCD]
```

The process $q\bar{q} \to ZH$ is calculated in the four flavour scheme (4FS), therefore a new particle `q` is defined including four light quark flavours. The two processes with `q q~` and `q~q` have to be considered. Omitting `[QCD]` defines the generation of $q\bar{q} \to ZH$ at LO.

```
> define q = u d c s
> define q~ = u~ d~ c~ s~
> generate q q~ > x0 l+ l- / a [QCD]
> add process q~ q > x0 l+ l- / a [QCD]
```

The output of the process generation is stored in a file which can then further be launched to generate the event. By directly editing general parameters and the parameter card, additional information can be passed during this step.

```
> output output_file
```

```
> launch output_file
> set nevents 10000
> set pdlabel lhapdf
> set lhaid 23300
> set cosa 1
> set ksm 1
> set kHtt 1
> set katt 0
```

During the parton shower which is performed using PYTHIA 8 [6], the scale of the partons is reduced from the scale of the hard interaction Q^2 down to the scale of hadronization Λ_{QCD} by radiating off particles. Until the infrared cutoff $Q_0^2 > \Lambda_{\mathrm{QCD}}$ is reached, the calculation is still in the perturbative regime. But reaching the soft regime with energies below Q_0^2 the perturbative expansion is no longer valid and models are needed to go to even lower momentum scales. Below the scale of strong interactions $\Lambda_{\mathrm{QCD}} \sim 1\,\mathrm{GeV}$ the process of hadronization dominates and quarks and gluons form hadrons. Decays into stable detectable particles are performed and particles are clustered to jets using FASTJET [21]. DELPHES 3 [7] is used as a detector simulation and for providing the object selection procedure, dealing with overlaps between objects. The b-tagging efficiency for DELPHES 3 is set to have a maximum value of 73 %. The data of the multiparticle final state then contains selected objects - electrons, muons, jets - which are then stored in ROOT [22] tree format.

3.2 Event Selection

To match the events which are generated by MADGRAPH5_AMC@NLO, PYTHIA 8 and DELPHES 3 as described in section 3.1, an event selection procedure similar to the one used on the experimental ATLAS data which is presented for example in [8] is performed on the data. We focus on the 2-lepton selection, because it has the best sensitivity to the $q\bar{q}$, $gg \to ZH$ processes. The event selection is summarized in table 3. It is implemented as a TSELECTOR class in ROOT.

Lepton Selection The Z boson is set to decay only into a pair of charged leptons. The variable `twoLeptons` is set to `True`, if a passed event does contain exactly these two leptons of the same flavour. For detectability, leptons are also required to be within a pseudorapitity range of $|\eta| < 2.47$ for electrons and $|\eta| < 2.7$ for muons and to have a transverse momentum larger than $p_T > 7\,\mathrm{GeV}$. If both leptons of one event do pass this selection and at least have one lepton has $p_T > 27\,\mathrm{GeV}$, `passLeptons` is set `True`. Andditionally, a cut on the reconstructed transverse momentum of the vector boson $p_T^V > 75\,\mathrm{GeV}$ is implemented. p_T^V can be calculated using the transverse momenta of the leptons $p_T^{V_i}$ and their corresponding azimuthal scattering angles ϕ_i

$$\begin{aligned} p_T^V &= \left|\vec{p}_T^{\,V_1} + \vec{p}_T^{\,V_2}\right| \\ &= \left|\begin{pmatrix} p_{T,1}\cos\phi_1 \\ p_{T,1}\sin\phi_1 \end{pmatrix} + \begin{pmatrix} p_{T,2}\cos\phi_2 \\ p_{T,2}\sin\phi_2 \end{pmatrix}\right| \\ &= \sqrt{\left(p_{T,1}\cos\phi_1 + p_{T,2}\cos\phi_2\right)^2 + \left(p_{T,1}\sin\phi_1 + p_{T,2}\sin\phi_2\right)^2}. \end{aligned} \tag{15}$$

Jet Selection The Higgs boson H is set to decay only into a pair of b quarks which then create exactly two b-tagged jets. This is ensured by the variable `twobJets`. At least one b-tagged jet is supposed to have a transverse momentum larger than 45 GeV, this status is stored in `PTofbJetGTR45`. Additional transverse momenta and pseudorapitity criteria are applied by `passJets`.

An Event does pass the event selection, if all variables are `True` after going through all leptons and jets,

```
passPreselectionLeptons = twoLeptons &&  passLeptons && PTofLeptonGTR27
passPreselectionJets = twobJets && PTofbJetGTR45 && passJets
passPreselection = passPreselectionLeptons && passPreselectionJets.
```

All cuts are summarized in table 3.

The tables 4-6 summarize the percentages of passed events after each cut for all seven studied CP mixing angles α. All results correspond to a size of $N = 50\,000$ generated events. Figure 2 shows cut flow diagrams for $\alpha = 0°$ and $\alpha = 90°$. The acceptance is slightly higher for $gg \to ZH$ for $\alpha = 90°$ than for $\alpha = 0°$. For $q\bar{q} \to ZH$ there is no significant difference between the acceptance for different CP mixing angles, because the Drell-Yan process is not affected by a BSM $Ht\bar{t}$ vertex. The lepton and jet cuts are independent from each other and do lower the acceptance close to the experimentally observed acceptances of 13.5 % for $gg \to ZH$ and 6 % for $q\bar{q} \to ZH$ [8]. The final acceptances after the process of event selection are summarized in table 7.

Figure 3 illustrates the calculated acceptance for different CP mixing angles compared to the experimental observation. The acceptance for $q\bar{q} \to ZH$ is independent of α and in agreement with the ATLAS result for NLO while the acceptance for the LO process is by 1.5 % too high. For $gg \to ZH$ the acceptance is in good agreement with the experimental result already for LO, but an enhancement with larger α is observed. This enhancement is due to the increasing cross section for $gg \to ZH$ with higher α which is further discussed in section 4.1. The acceptance for $\alpha = 180°$ is 2 % larger than for the SM $\alpha = 0°$ case.

Table 3: Cuts for event selection

Category	description	variable name
Leptons	exactly 2 leptons of the same flavour	`twoLeptons`
	$p_{T,\text{elec}} > 7\,\text{GeV}$ and $\lvert\eta_{\text{elec}}\rvert < 2.47$ $p_{T,\text{muon}} > 7\,\text{GeV}$ and $\lvert\eta_{\text{muon}}\rvert < 2.7$ $p_{T,\text{leading}} > 27\,\text{GeV}$	`passLeptons`
Jets	exactly 2 b-tagged jets	`twobJets`
	at least one b-tagged jet with $p_{T,\text{leading}} > 45\,\text{GeV}$	`PTofbJetGTR45`
	$p_T > 20\,\text{GeV}$ and $\lvert\eta\rvert < 2.5$ $p_T > 30\,\text{GeV}$ and $2.5 < \lvert\eta\rvert < 4.5$	`passJets`

Table 4: Cut flow data for $gg \to ZH$ with statistical errors

	$gg \to ZH$ [LO]						
Cut \ α	0°	18°	45°	72°	90°	135°	180°
twoLeptons	56.9 ± 0.3	57.1 ± 0.3	58.3 ± 0.3	59.1 ± 0.3	58.8 ± 0.3	59.9 ± 0.3	59.5 ± 0.3
passLeptons	49.4 ± 0.3	49.8 ± 0.3	52.2 ± 0.3	54.1 ± 0.3	53.9 ± 0.3	55.5 ± 0.3	55.2 ± 0.3
twobJets	15.2 ± 0.2	15.7 ± 0.2	16.3 ± 0.2	17.0 ± 0.2	17.1 ± 0.2	17.5 ± 0.2	17.7 ± 0.2
PTofbJetGTR45	14.8 ± 0.2	15.3 ± 0.2	16.0 ± 0.2	16.7 ± 0.2	16.8 ± 0.2	17.2 ± 0.2	17.4 ± 0.2
passJets	12.6 ± 0.2	13.0 ± 0.2	13.5 ± 0.2	14.1 ± 0.2	14.2 ± 0.2	14.6 ± 0.2	14.7 ± 0.2

Table 5: Cut flow data for $q\bar{q} \to ZH$ [LO] with statistical errors

	$q\bar{q} \to ZH$ [LO]						
Cut \ α	0°	18°	45°	72°	90°	135°	180°
twoLeptons	51.7 ± 0.3	51.9 ± 0.3	51.3 ± 0.3	51.2 ± 0.3	51.1 ± 0.3	51.6 ± 0.3	51.7 ± 0.3
passLeptons	29.3 ± 0.2	29.5 ± 0.2	29.0 ± 0.2	29.1 ± 0.2	28.7 ± 0.2	29.1 ± 0.2	29.4 ± 0.2
twobJets	8.3 ± 0.1	8.4 ± 0.1	8.3 ± 0.1	8.3 ± 0.1	8.1 ± 0.1	8.5 ± 0.1	8.4 ± 0.1
PTofbJetGTR45	8.0 ± 0.1	8.1 ± 0.1	8.1 ± 0.1	8.0 ± 0.1	7.9 ± 0.1	8.2 ± 0.1	8.0 ± 0.1
passJets	7.4 ± 0.1	7.5 ± 0.1	7.4 ± 0.1	7.4 ± 0.1	7.2 ± 0.1	7.6 ± 0.1	7.4 ± 0.1

Table 6: Cut flow data for $q\bar{q} \to ZH$ [NLO] with statistical errors

	$q\bar{q} \to ZH$ [NLO]						
Cut \ α	0°	18°	45°	72°	90°	135°	180°
twoLeptons	42.0 ± 0.3	42.4 ± 0.3	41.8 ± 0.3	42.1 ± 0.3	42.1 ± 0.3	42.3 ± 0.3	42.1 ± 0.3
passLeptons	23.3 ± 0.2	23.5 ± 0.2	22.9 ± 0.2	23.2 ± 0.2	23.2 ± 0.2	23.6 ± 0.2	23.2 ± 0.2
twobJets	6.7 ± 0.1	6.6 ± 0.1	6.4 ± 0.1	6.4 ± 0.1	6.6 ± 0.1	6.5 ± 0.1	6.5 ± 0.1
PTofbJetGTR45	6.4 ± 0.1	6.4 ± 0.1	6.2 ± 0.1	6.2 ± 0.1	6.4 ± 0.1	6.2 ± 0.1	6.3 ± 0.1
passJets	6.1 ± 0.1	6.1 ± 0.1	5.9 ± 0.1	5.9 ± 0.1	6.1 ± 0.1	5.9 ± 0.1	6.0 ± 0.1

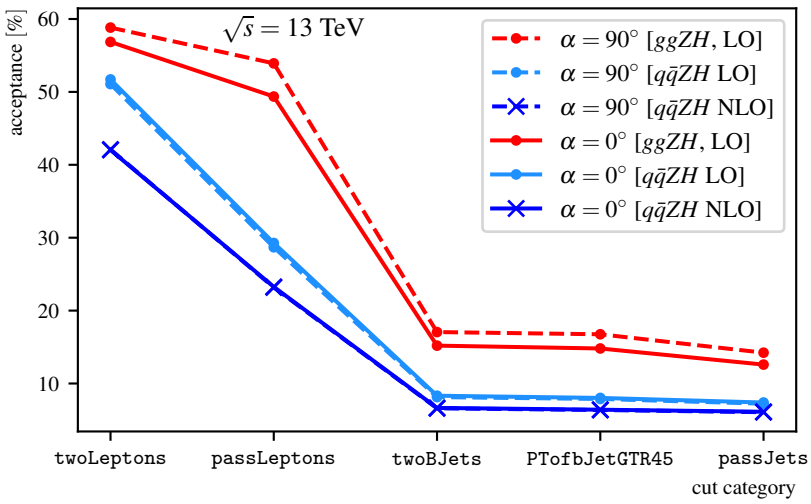

Figure 2: Cut flow diagram for $\alpha = 0°$ and $\alpha = 90°$

Table 7: Event data acceptance

Process	exp [%]	$\alpha = 0°$ [%]	$\alpha = 18°$ [%]	$\alpha = 45°$ [%]	$\alpha = 72°$ [%]	$\alpha = 90°$ [%]	$\alpha = 135°$ [%]	$\alpha = 180°$ [%]
$gg \to ZH \to llb\bar{b}$ [LO]	13.5	12.6 ± 0.2	13.0 ± 0.2	13.5 ± 0.2	14.1 ± 0.2	14.2 ± 0.2	14.6 ± 2.0	14.7 ± 0.2
$q\bar{q} \to ZH \to llb\bar{b}$ [LO]	6.0	7.4 ± 0.1	7.5 ± 0.1	7.4 ± 0.1	7.4 ± 0.1	7.2 ± 0.1	7.6 ± 0.1	7.4 ± 0.1
$q\bar{q} \to ZH \to llb\bar{b}$ [NLO]	6.0	6.1 ± 0.1	6.1 ± 0.1	6.0 ± 0.1	5.9 ± 0.1	6.1 ± 0.1	6.0 ± 0.1	6.0 ± 0.1

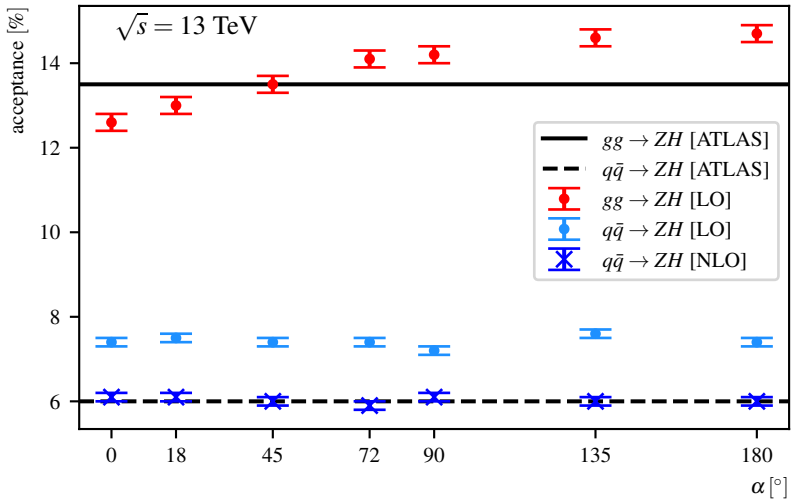

Figure 3: Comparison of calculated acceptances after applying cuts and experimental data [8]

4 Discussion

After event generation and selection the obtained data set is further studied in terms of the calculated cross sections in section 4.1, the distribution of observables in section 4.2, signal yield in section 4.3 and signal strength in section 4.4.

4.1 Cross Sections

Table 8 does summarize the cross sections for 10 000 and 50 000 events and all seven CP mixing angles α which were calculated by the MadGraph5_aMC@NLO framework described in section 3.

The data for $q\bar{q} \to ZH$ shows no variation beyond the statistical fluctuation for the cross section for different α. The medium cross section for the leading order process is 25.28 fb, for the next-to-leading order process the cross section is on average 48.75 fb. The NLO result agrees with the precision result presented in [23], $\sigma^{q\bar{q}ZH}_{\text{NLO+NNL}} = 51.36^{+3.8}_{-3.1}$fb, which is also visible in figure 4. The reason for the α-independence of the qq-cross section is that the Drell-Yan Process dominates the cross section and the changed CP character does only enter the couplings to $Ht\bar{t}$ vertices.

The $Ht\bar{t}$ vertices are a part of the box type diagrams for the $gg \to ZH$ process and lead to a significant change in the calculated cross section. A larger mixing angle α leads to an increase of the cross section. The cross section for $\alpha = 180°$ is 10 fb larger than the cross section for $\alpha = 0°$. The calculated cross section agrees with the precision result presented in [23], $\sigma^{ggZH}_{\text{NLO+NNL}} = 4.14^{+3.8}_{-3.1}$fb for $\alpha \leq 90°$.

Table 8: Cross sections

Process	N [10^3]	$\alpha = 0°$ [fb]	$\alpha = 18°$ [fb]	$\alpha = 45°$ [fb]	$\alpha = 72°$ [fb]	$\alpha = 90°$ [fb]	$\alpha = 135°$ [fb]	$\alpha = 180°$ [fb]
$gg \to ZH \to llb\bar{b}$ [LO]	10	2.58 ± 0.02	2.87 ± 0.02	4.114 ± 0.009	6.16 ± 0.02	7.75 ± 0.04	11.19 ± 0.09	12.50 ± 0.03
	50	2.577 ± 0.008	2.851 ± 0.002	4.13 ± 0.01	6.13 ± 0.02	7.71 ± 0.01	11.24 ± 0.03	12.57 ± 0.04
$q\bar{q} \to ZH \to llb\bar{b}$ [LO]	10	25.14 ± 0.05	25.16 ± 0.05	25.40 ± 0.05	25.30 ± 0.04	25.32 ± 0.04	25.34 ± 0.03	25.28 ± 0.04
	50	25.28 ± 0.02	25.28 ± 0.02	25.30 ± 0.02	25.26 ± 0.02	25.34 ± 0.02	25.22 ± 0.02	25.26 ± 0.02
$q\bar{q} \to ZH \to llb\bar{b}$ [NLO]	10	48.65 ± 0.08	48.66 ± 0.08	48.74 ± 0.08	48.70 ± 0.07	48.66 ± 0.07	48.79 ± 0.08	48.70 ± 0.07
	50	48.70 ± 0.08	48.69 ± 0.07	48.85 ± 0.08	48.86 ± 0.07	48.71 ± 0.08	48.76 ± 0.08	48.68 ± 0.07

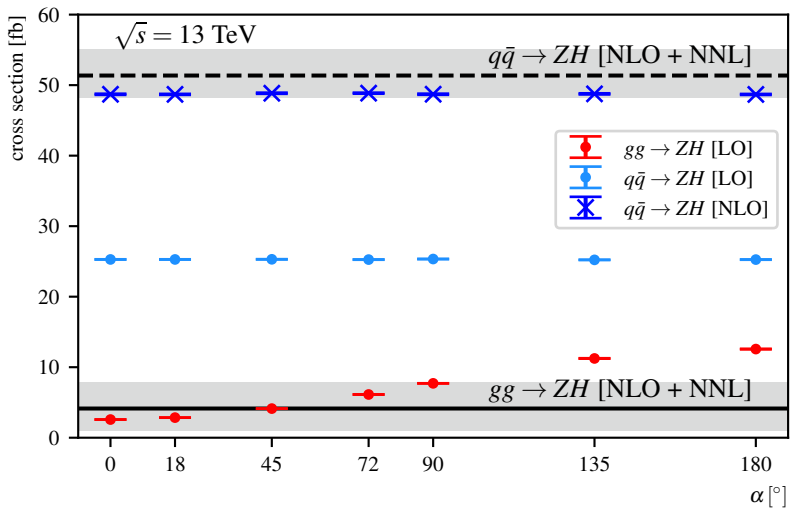

Figure 4: Comparison of calculated cross sections with precision results from [23]

4.2 Comparison of Observables

The following section is aimed at the visualization of the distributions of observables with emphasis on the effects of a variation of α.

Figure 5 and 6 illustrate the distribution of the b-tagged jet invariant mass M_{bb} and the lepton invariant mass M_{ll}. The lower pad illustrates the ratio between $\alpha = 0°$ and $\alpha = 90°$. M_{ll} and M_{bb} are calculated from the momentum four-vectors defined using the `TLorentzVector` class of `ROOT`. The distributions are almost independent of the CP mixing angle α. M_{bb} shows a peak around 110 GeV. Due to energy loss in the b jets, it is slightly off the measured Higgs mass of 125 GeV. M_{ll} peaks at 91 GeV, the mass of the Z boson. Because of high detection efficiency for the leptons, the peak in the invariant lepton mass shows almost no deviations from the Z boson mass.

Figure 7, 13 and 19 show the reconstructed transverse momentum of the b-tagged jets which is calculated according to equation (15). For $gg \to ZH$ the p_T spectrum shifts to higher p_T values for an increasing α. For $q\bar{q} \to ZH$ a variation of α does not change the p_T distribution. This observation is also made for the reconstructed p_T of the Z boson, displayed in figures 8, 14 and 20. The distribution of the p_T of the leading lepton, displayed in figures 9, 15 and 21 and the leading b jet, displayed in figures 11, 17 and 23, do also show a harder spectrum for larger α only for the $gg \to ZH$ process.

The distribution of the number of jets, displayed in figures 10, 16 and 22 and the p_T of the subleading jet, displayed in figures 12, 18 and 24, do not show a significant difference between different CP mixing angles α.

Process $gg \to ZH$

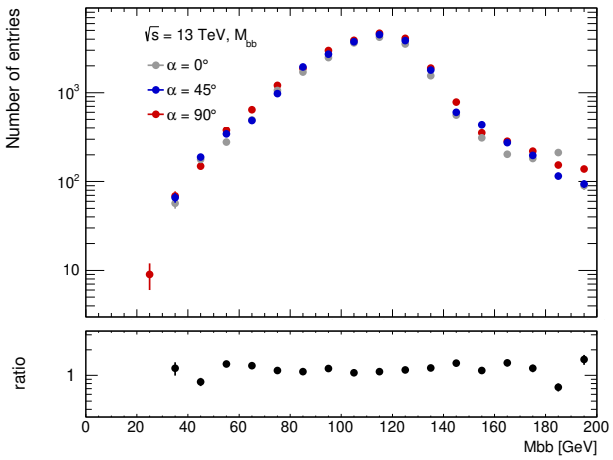

Figure 5: b-tagged jets invariant mass M_{bb}

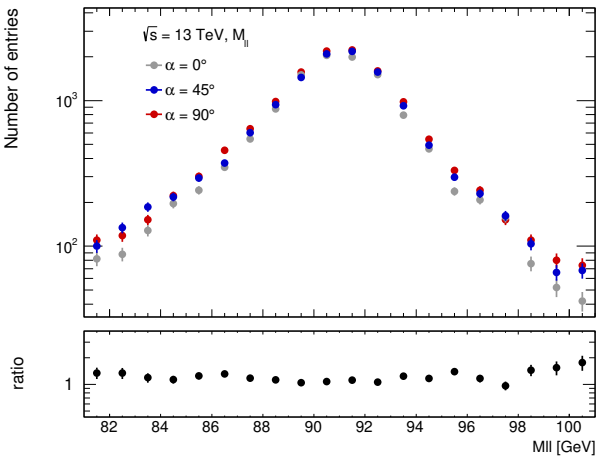

Figure 6: Lepton invariant mass M_{ll}

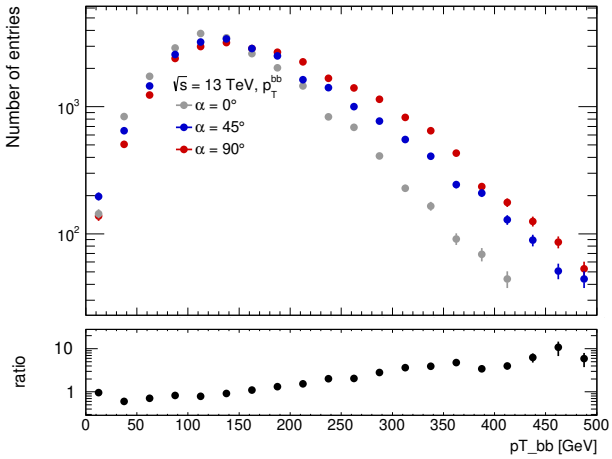

Figure 7: Reconstructed p_T of the Higgs boson

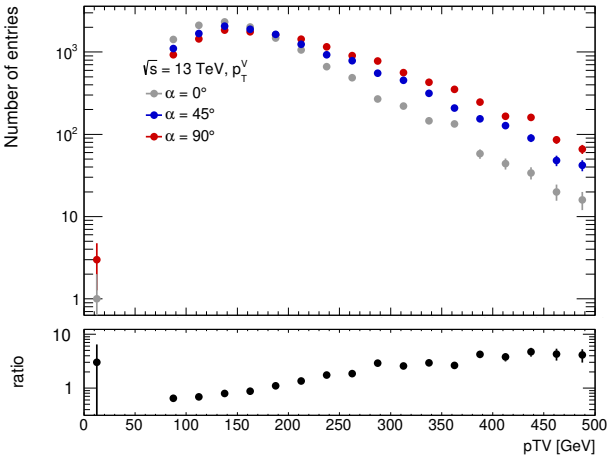

Figure 8: Reconstructed p_T of the Z boson

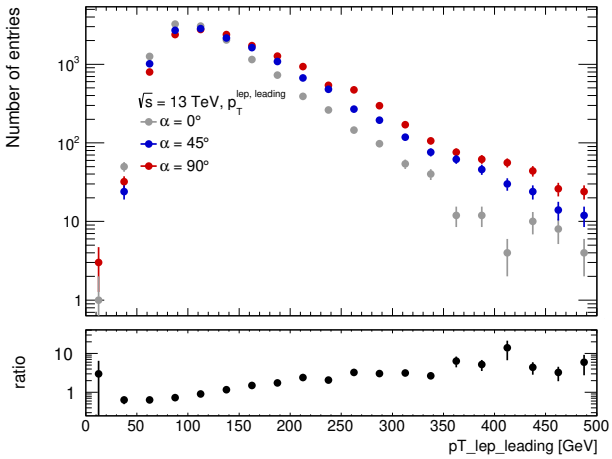

Figure 9: p_T of the leading lepton

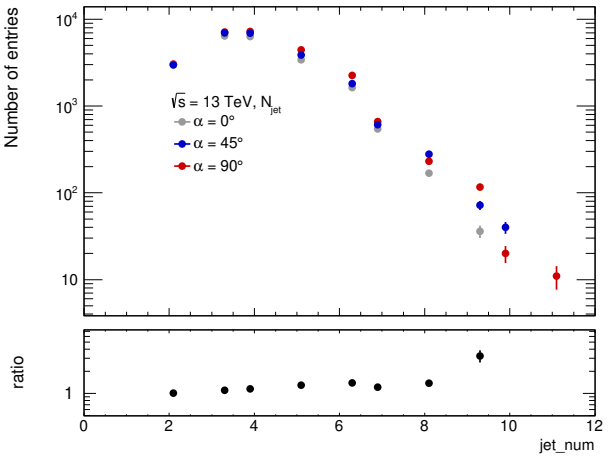

Figure 10: Number of jets

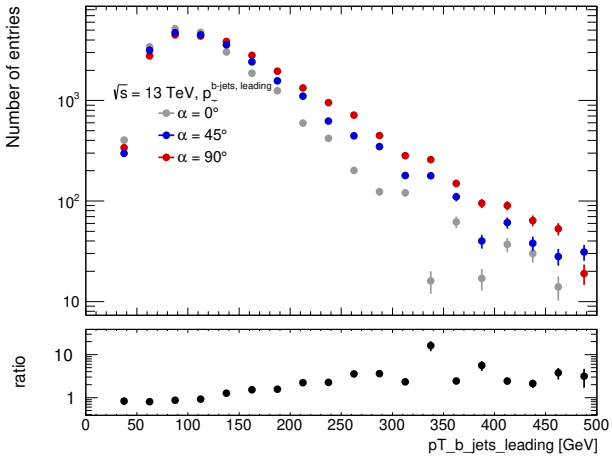

Figure 11: p_T of the leading b jet

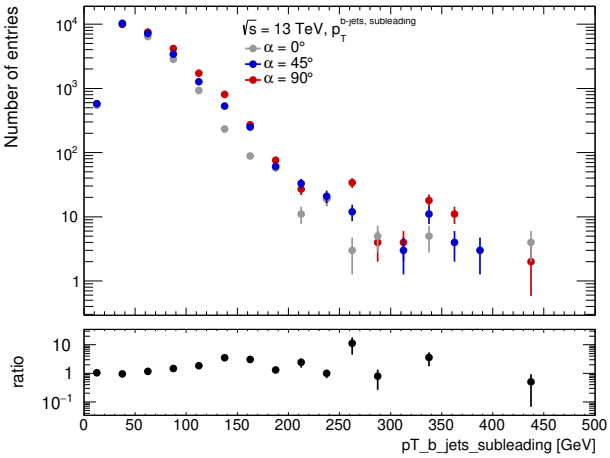

Figure 12: p_T of the subleading b jet

Process $q\bar{q} \to ZH$ [LO]

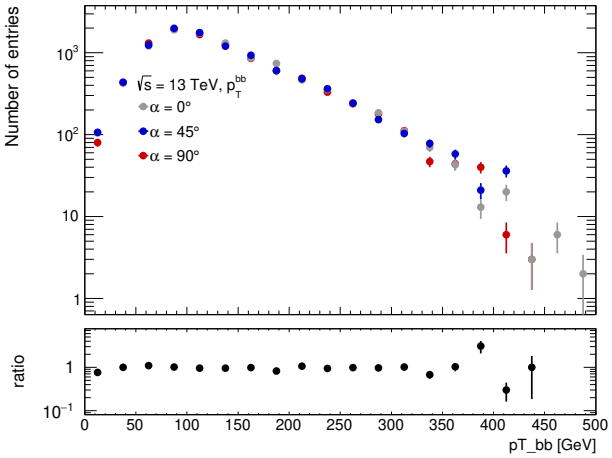

Figure 13: Reconstructed p_T of the Higgs boson

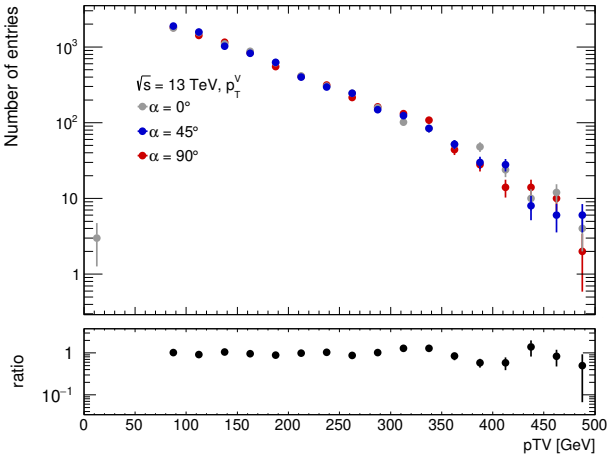

Figure 14: Reconstructed p_T of the Z boson

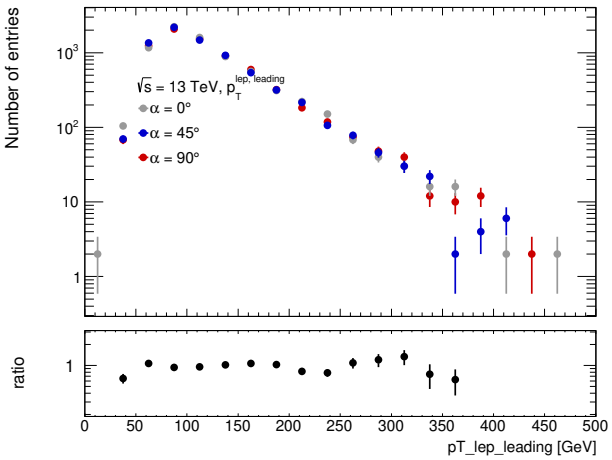

Figure 15: p_T of the leading lepton

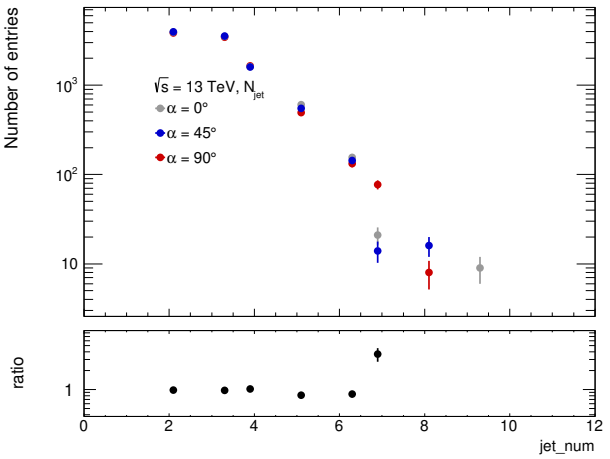

Figure 16: Number of jets

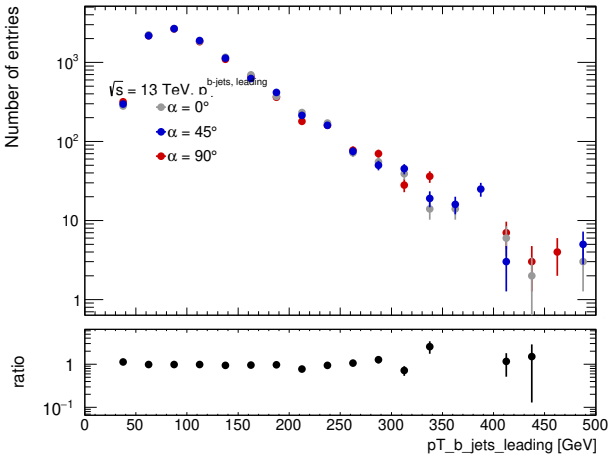

Figure 17: p_T of the leading b jet

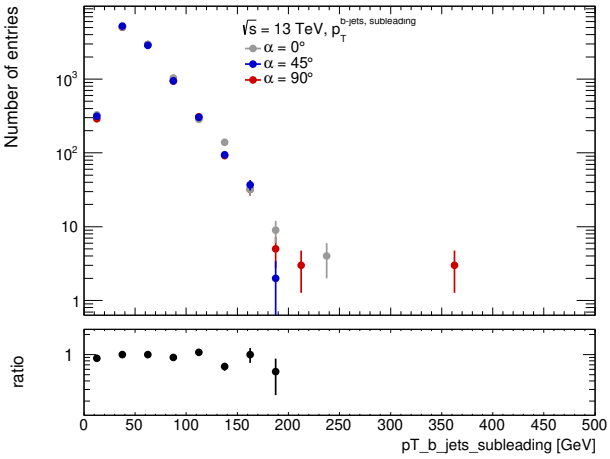

Figure 18: p_T of the subleading b jet

Process $q\bar{q} \to ZH$ [NLO]

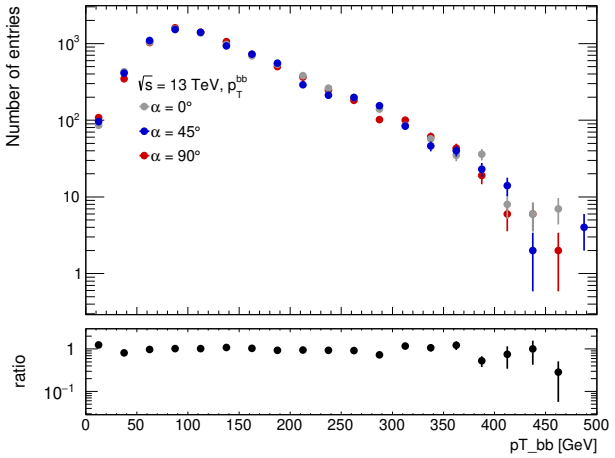

Figure 19: Reconstructed p_T of the Higgs boson

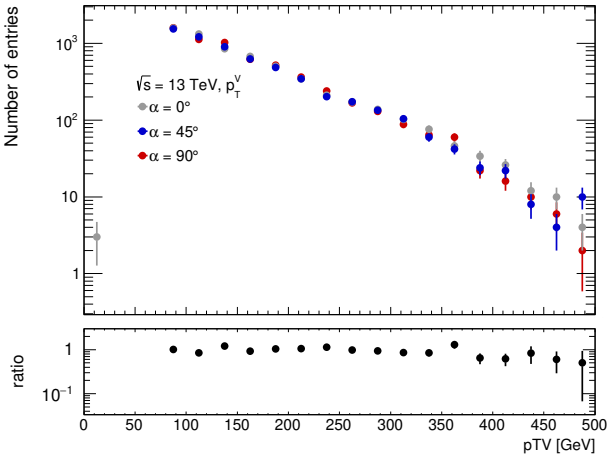

Figure 20: Reconstructed p_T of the Z boson

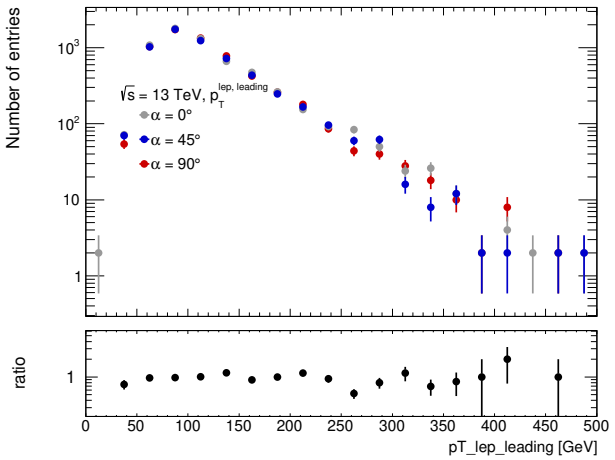

Figure 21: p_T of the leading lepton

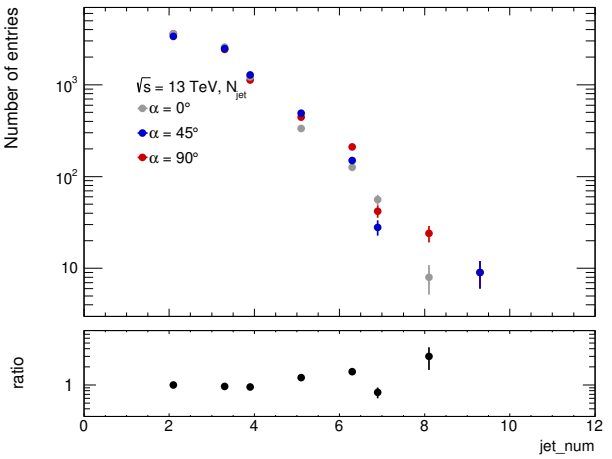

Figure 22: Number of jets

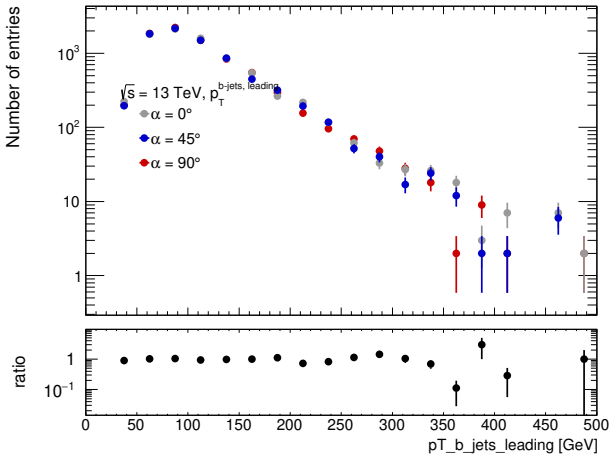

Figure 23: p_T of the leading b jet

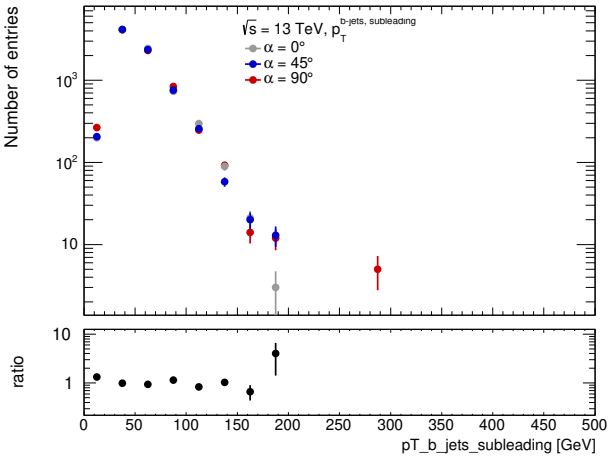

Figure 24: p_T of the subleading b jet

4.3 Signal Yield

Following [8] the events which passed the event selection are sorted into four signal categories.

1. All events with exactly two jets, which must then also be b-tagged. Additionally, the reconstructed transverse momentum of the vector boson is in the medium range of $75\,\text{GeV} < p_T^V < 150\,\text{GeV}$.
2. Events with $75\,\text{GeV} < p_T^V < 150\,\text{GeV}$, but with three or more jets.
3. Events with exactly two b-tagged jets which fall in the high p_T^V range with $p_T^V > 150\,\text{GeV}$.
4. Events with $p_T^V > 150\,\text{GeV}$, but with three or more jets.

The calculated acceptances per signal region for all seven CP mixing angles α are displayed in table 9

The signal yield N_S^i for a signal category i, with $i \in \{1, 2, 3, 4\}$ is calculated as

$$N_S^i = \int dt\mathcal{L} \cdot \left[\epsilon^i_{ggZH}\widetilde{\sigma}_{ggZH} + \epsilon^i_{q\bar{q}ZH}\widetilde{\sigma}_{q\bar{q}ZH}\right] \cdot BR(H \to b\bar{b}) \tag{16}$$

with the integrated luminosity $\int dt\mathcal{L} = 79.8\,\text{fb}^{-1}$ [8], the acceptance for each category $\epsilon^i = \frac{N_{\text{passed}}}{N_{\text{tot}}}$, the branching ratio $BR(H \to b\bar{b}) = 0.58$ [23] and

$$\widetilde{\sigma} = \frac{\sigma^{\text{model}}_{\text{MC}}}{\sigma^{\text{SM}}_{\text{MC}}} \cdot \sigma^{\text{SM}}_{\text{precision}}. \tag{17}$$

Where $\sigma^{\text{SM}}_{\text{precision}}$ corresponds to the precision results from [23]

$$\sigma^{gg\to ZH\,,\,\text{SM}}_{\text{precision, NLO+NNL}} = 4.14\,^{+3.8}_{-3.1}\,\text{fb} \tag{18}$$

$$\sigma^{q\bar{q}\to ZH\,,\,\text{SM}}_{\text{precision, NLO+NNL}} = 51.36\,^{+3.8}_{-3.1}\,\text{fb}. \tag{19}$$

The figures 25-28 show the calculated signal yields for LO and NLO $q\bar{q} \to ZH$ results with statistical errors for the four signal regions. The calculated signal yield is observed to increase with higher α for all signal regions. For 2 jets the signal yield is slightly higher then the experimental result, but still within the 1σ confidence level. For 3 and more jets the signal yield is lower than the experimental result and outside the 1σ confidence level for $\alpha = 0°$, though there are only purely statistical errors considered.

Table 9: Acceptance per signal region for 50 000 generated events

Process		$75\,\text{GeV} < p_T^V < 150\,\text{GeV}$		$p_T^V > 150\,\text{GeV}$	
		2-jet	3-jet	2-jet	3-jet
			$\alpha = 0°$		
$gg \to ZH \to llb\bar{b}$	[LO]	1.66 ± 0.06	4.22 ± 0.09	1.36 ± 0.05	5.4 ± 0.1
$q\bar{q} \to ZH \to llb\bar{b}$	[LO]	2.48 ± 0.07	1.94 ± 0.06	1.45 ± 0.05	1.52 ± 0.06
$q\bar{q} \to ZH \to llb\bar{b}$	[NLO]	2.27 ± 0.07	1.49 ± 0.05	1.33 ± 0.05	1.04 ± 0.05
			$\alpha = 18°$		
$gg \to ZH \to llb\bar{b}$	[LO]	1.75 ± 0.06	4.0 ± 0.1	1.40 ± 0.05	5.8 ± 0.1
$q\bar{q} \to ZH \to llb\bar{b}$	[LO]	2.44 ± 0.07	2.01 ± 0.06	1.51 ± 0.05	1.49 ± 0.05
$q\bar{q} \to ZH \to llb\bar{b}$	[NLO]	2.29 ± 0.07	1.39 ± 0.05	1.28 ± 0.05	1.10 ± 0.05
			$\alpha = 45°$		
$gg \to ZH \to llb\bar{b}$	[LO]	1.29 ± 0.05	3.56 ± 0.08	1.69 ± 0.06	7.0 ± 0.1
$q\bar{q} \to ZH \to llb\bar{b}$	[LO]	2.54 ± 0.07	1.96 ± 0.06	1.41 ± 0.05	1.48 ± 0.05
$q\bar{q} \to ZH \to llb\bar{b}$	[NLO]	2.23 ± 0.07	1.43 ± 0.05	1.14 ± 0.05	1.12 ± 0.05
			$\alpha = 72°$		
$gg \to ZH \to llb\bar{b}$	[LO]	1.19 ± 0.05	3.32 ± 0.08	1.88 ± 0.06	7.7 ± 0.1
$q\bar{q} \to ZH \to llb\bar{b}$	[LO]	2.42 ± 0.07	1.99 ± 0.06	1.47 ± 0.05	1.51 ± 0.06
$q\bar{q} \to ZH \to llb\bar{b}$	[NLO]	2.26 ± 0.07	1.39 ± 0.05	1.19 ± 0.05	1.06 ± 0.05
			$\alpha = 90°$		
$gg \to ZH \to llb\bar{b}$	[LO]	1.11 ± 0.05	3.12 ± 0.08	1.94 ± 0.06	8.1 ± 0.1
$q\bar{q} \to ZH \to llb\bar{b}$	[LO]	2.47 ± 0.07	1.91 ± 0.06	1.37 ± 0.05	1.47 ± 0.05
$q\bar{q} \to ZH \to llb\bar{b}$	[NLO]	2.31 ± 0.07	1.42 ± 0.05	1.29 ± 0.05	1.03 ± 0.05
			$\alpha = 135°$		
$gg \to ZH \to llb\bar{b}$	[LO]	1.06 ± 0.05	3.08 ± 0.08	2.05 ± 0.06	8.4 ± 0.1
$q\bar{q} \to ZH \to llb\bar{b}$	[LO]	2.53 ± 0.07	2.08 ± 0.06	1.46 ± 0.05	1.53 ± 0.06
$q\bar{q} \to ZH \to llb\bar{b}$	[NLO]	2.16 ± 0.07	1.44 ± 0.05	1.25 ± 0.05	1.08 ± 0.05
			$\alpha = 180°$		
$gg \to ZH \to llb\bar{b}$	[LO]	1.05 ± 0.05	3.01 ± 0.08	2.08 ± 0.06	8.5 ± 0.1
$q\bar{q} \to ZH \to llb\bar{b}$	[LO]	2.50 ± 0.07	1.97 ± 0.06	1.38 ± 0.05	1.58 ± 0.06
$q\bar{q} \to ZH \to llb\bar{b}$	[NLO]	2.21 ± 0.07	1.39 ± 0.05	1.33 ± 0.05	1.05 ± 0.05

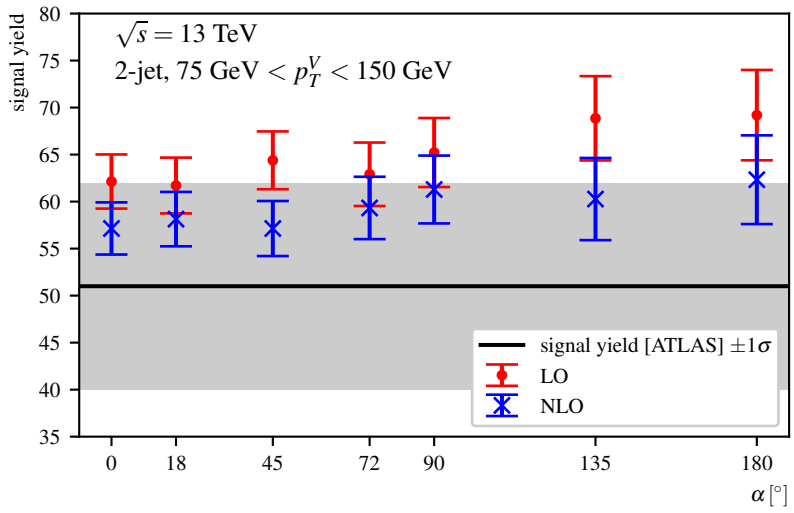

Figure 25: Calculated signal yield for 2-jet and 75 GeV $< p_T^V <$ 150 GeV with statistical errors compared with experimental data from [8, 23]

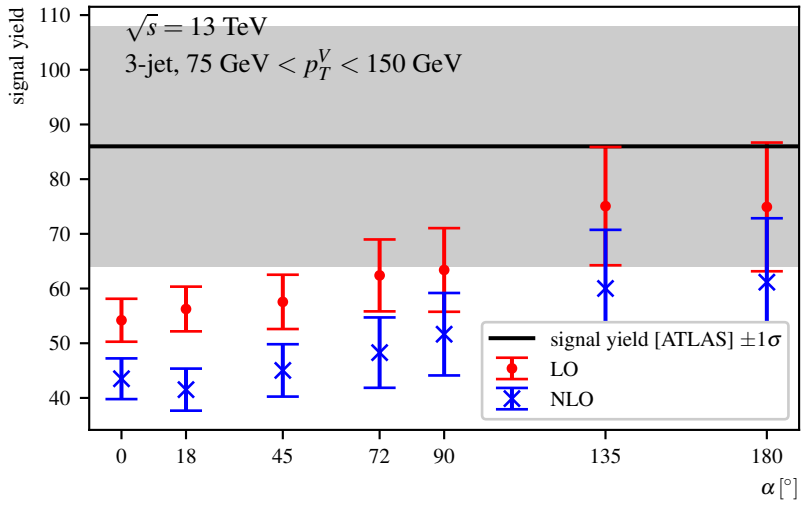

Figure 26: Calculated signal yield for 3-jet and 75 GeV $< p_T^V <$ 150 GeV with statistical errors compared with experimental data from [8, 23]

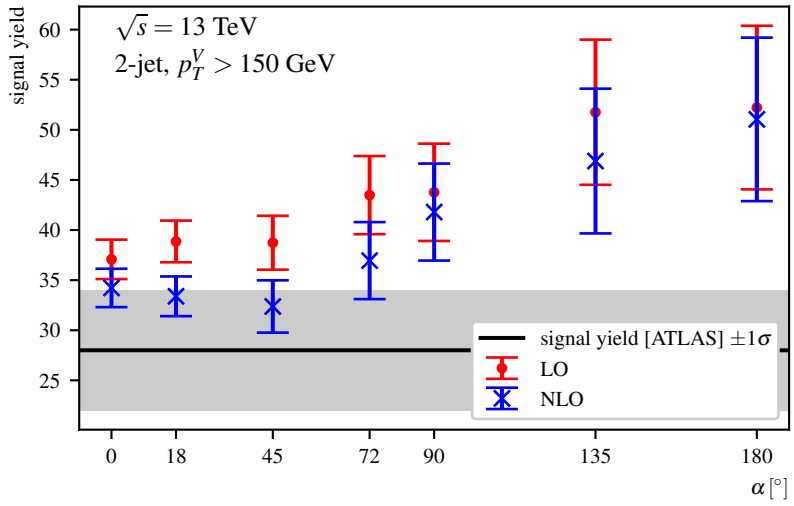

Figure 27: Calculated signal yield for 2-jet and $p_T^V > 150\,\text{GeV}$ with statistical errors compared with experimental data from [8, 23]

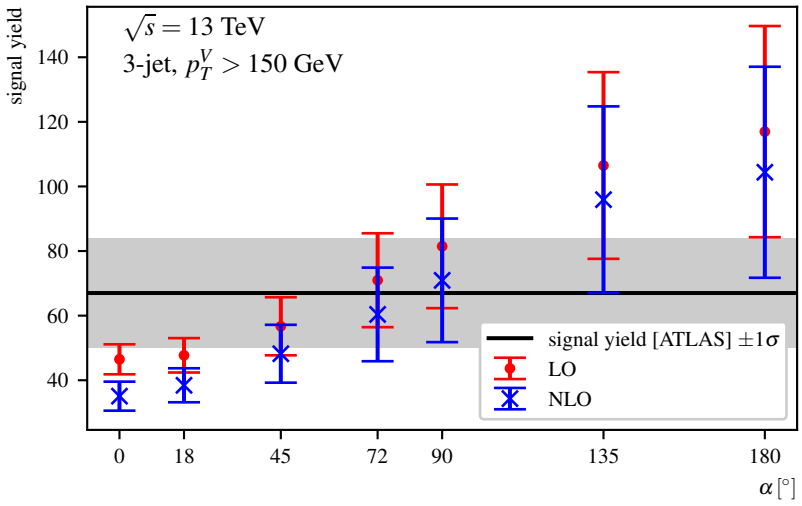

Figure 28: Calculated signal yield for 3-jet and $p_T^V > 150\,\text{GeV}$ with statistical errors compared with experimental data from [8, 23]

4.4 Signal Strength

The signal strength μ is calculated as the predicted rate normalized by the SM rate

$$\mu = \frac{\sum_i \epsilon_i(\alpha)\sigma_i(\alpha) \times BR\left(H \to b\bar{b}\right)}{\sum_i \epsilon_i^{SM}\sigma_i^{SM} \times BR^{SM}(H \to b\bar{b})} \tag{20}$$

with $i \in \{q\bar{q} \to ZH, gg \to ZH\}$. Assuming that the branching ratio of the Higgs decay is not affected by a BSM coupling

$$BR(H \to b\bar{b}) \equiv BR^{SM}(H \to b\bar{b}) \tag{21}$$

the signal strength reads

$$\mu = \frac{\sum_i \epsilon_i(\alpha)\sigma_i(\alpha)}{\sum_i \epsilon_i^{SM}\sigma_i^{SM}}, \quad i \in \{q\bar{q} \to ZH, gg \to ZH\} \tag{22}$$

$$= \frac{\epsilon_{q\bar{q}ZH}(\alpha)\sigma_{q\bar{q}ZH}(\alpha) + \epsilon_{ggZH}(\alpha)\sigma_{ggZH}(\alpha)}{\epsilon^{SM}_{q\bar{q}ZH}\sigma^{SM}_{q\bar{q}ZH} + \epsilon^{SM}_{ggZH}\sigma^{SM}_{ggZH}}. \tag{23}$$

Figure 29 shows a significant increase of the signal strength with increasing α. For $\alpha \leq 90°$ the calculated signal strength is in agreement with the experimental result for the combined W and Z boson associated Higgs production, $\mu_{\text{exp},VH}$. For $\alpha = 135°$ only the NLO calculation result is in agreement with $\mu_{\text{exp},VH}$. All calculated signal strengths are within the errorband of the experimental signal strength of $pp \to Z(\to l^+l^-)H$, $\mu_{\text{exp},2L}$.

Plotting the signal strength μ inserting only SM acceptances, as it is displayed in figure 30, does not significantly change the plot. μ does increase in total because of the increasing cross section for $gg \to ZH$, but the effect of a different acceptance is not relevant.

The focus of the used MadGraph5_aMC@NLO framework, which was introduced in section 4, is not on giving the most accurate results for the cross section. By rescaling the cross section with the parameter κ_i which is defined as the ratio of the precision SM cross section from [23] and the result for the SM cross section from Monte Carlo simulation

$$\kappa_i = \frac{\sigma_i^{\text{SM, prec}}}{\sigma_i^{\text{SM, MC}}}, \quad i \in \{q\bar{q} \to ZH, gg \to ZH\} \tag{24}$$

inaccuracies from the Monte Carlo simulations are levelled out. The calculated values for κ are displayed in table 10. Figure 10 shows the signal strength rescaled by the κ parameter.

Table 10: Cross section rescaling parameter κ

	$gg \to ZH \to l\bar{l}b\bar{b}$ [LO]	$q\bar{q} \to ZH \to l\bar{l}b\bar{b}$ [LO]	$q\bar{q} \to ZH \to l\bar{l}b\bar{b}$ [NLO]
κ_i	1.607	2.032	1.055

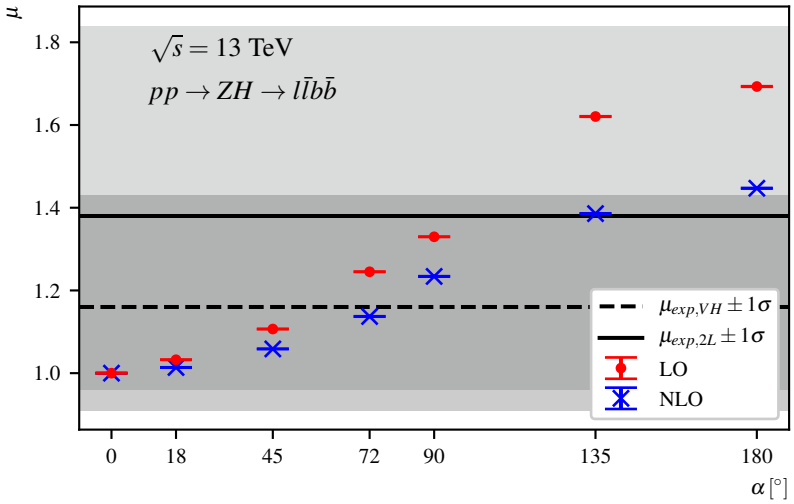

Figure 29: Calculated signal strength for different values of α compared with experimental result [8]

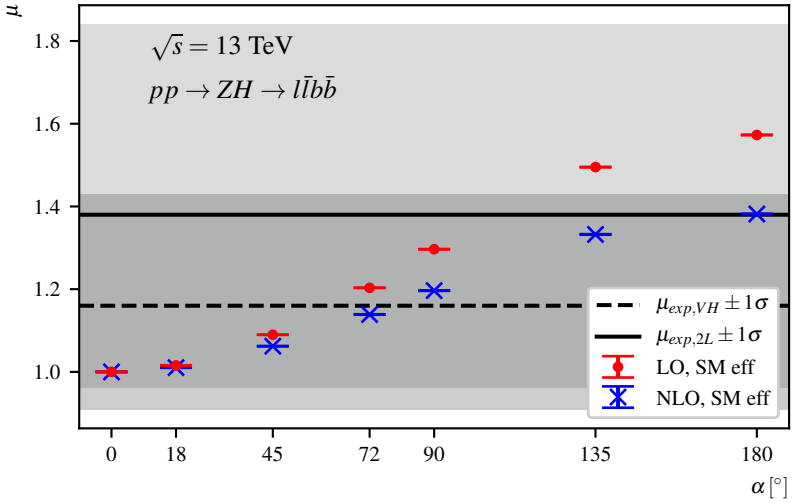

Figure 30: Signal strength using only the acceptance for $\alpha = 0°$

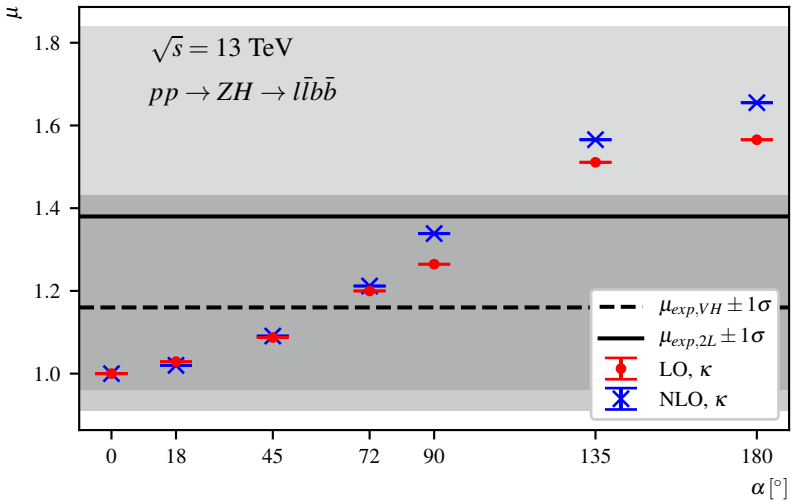

Figure 31: Signal strength with rescaled cross section

5 Summary

The process of Higgs production in association with a Z boson is sensitive to a CP odd component of the $Ht\bar{t}$ coupling.

The quark induced Z associated production shows no significant dependence of α. It is dominated by the Drell-Yan Process with no $Ht\bar{t}$ interaction involved in the hard scattering process.

On the other hand, the gluon induced process shows a dependence of α. For the Standard Model CP even Higgs boson, box diagrams with a $Ht\bar{t}$ vertex and triangle loop diagrams with a HZZ vertex do interfere destructively. Raising α to non-zero angles does lead to constructive interference between those two groups of contributing diagrams. Larger α lead to an increase of the total cross section for $gg \to ZH$, the overall detection sensitivity is therefore also raised. The reconstructed p_T of the Higgs and the Z boson, as well as the p_T of the leading lepton and the leading b-tagged jet are shifted towards higher momenta.

The calculated signal strength is still within the experimental errorband for the Z associated production, but is predicted to increase its value when α is raised within the considered range $\alpha \in [0°, 180°]$. The signal yields for the four signal regions do also increase with higher α. What is still to be understood is the difference in the calculated signal yields between 2-jet and 3-jet categories. A further cross check with ATLAS results for vector boson associated Higgs production with $H \to b\bar{b}$ within the simplified template cross-section framework [24] could be a possible next step.

Acknowledgments

This work was done during the 2019 summer student program at the DESY theory group in Hamburg. I would like to thank Dieter Zeppenfeld and Stefan Liebler for their recommendation and for originally drawing my attention to the program. My sincere thanks goes to Georg Weiglein for providing me this unique opportunity and for his supervision. Thanks to Tim Stefaniak and Henning Bahl for their guidance and always competent answers. Thanks to Matthias Saimpert for providing programming support and giving further impulses.

References

[1] Georges Aad et al. "Observation of a new particle in the search for the Standard Model Higgs boson with the ATLAS detector at the LHC". In: *Phys. Lett.* B716 (2012), pp. 1–29. DOI: 10.1016/j.physletb.2012.08.020. arXiv: 1207.7214 [hep-ex].

[2] Serguei Chatrchyan et al. "Observation of a New Boson at a Mass of 125 GeV with the CMS Experiment at the LHC". In: *Phys. Lett.* B716 (2012), pp. 30–61. DOI: 10.1016/j.physletb.2012.08.021. arXiv: 1207.7235 [hep-ex].

[3] Georges Aad et al. "Measurements of Higgs boson production and couplings in diboson final states with the ATLAS detector at the LHC". In: *Phys. Lett.* B726 (2013). [Erratum: Phys. Lett.B734,406(2014)], pp. 88–119. DOI: 10.1016/j.physletb.2014.05.011,10.1016/j.physletb.2013.08.010. arXiv: 1307.1427 [hep-ex].

[4] CMS Collaboration. "Measurement of the properties of a Higgs boson in the four-lepton final state". In: *Phys. Rev. D* 89 (9 May 2014), p. 092007. DOI: 10.1103/PhysRevD.89.092007. URL: https://link.aps.org/doi/10.1103/PhysRevD.89.092007.

[5] J. Alwall et al. "The automated computation of tree-level and next-to-leading order differential cross sections, and their matching to parton shower simulations". In: *JHEP* 07 (2014), p. 079. DOI: 10.1007/JHEP07(2014)079. arXiv: 1405.0301 [hep-ph].

[6] Torbjörn Sjöstrand et al. "An Introduction to PYTHIA 8.2". In: *Comput. Phys. Commun.* 191 (2015), pp. 159–177. DOI: 10.1016/j.cpc.2015.01.024. arXiv: 1410.3012 [hep-ph].

[7] J. de Favereau et al. "DELPHES 3, A modular framework for fast simulation of a generic collider experiment". In: *JHEP* 02 (2014), p. 057. DOI: 10.1007/JHEP02(2014)057. arXiv: 1307.6346 [hep-ex].

[8] Morad Aaboud et al. "Observation of $H \to b\bar{b}$ decays and VH production with the ATLAS detector". In: *Phys. Lett.* B786 (2018), pp. 59–86. DOI: 10.1016/j.physletb.2018.09.013. arXiv: 1808.08238 [hep-ex].

[9] P. Artoisenet et al. "A framework for Higgs characterisation". In: *JHEP* 11 (2013), p. 043. DOI: 10.1007/JHEP11(2013)043. arXiv: 1306.6464 [hep-ph].

[10] Michael Edward [VerfasserIn] Peskin. *An introduction to quantum field theory*. Ed. by Daniel V. [VerfasserIn] Schroeder. Student economy. The advanced book program. [Boulder]: Westview Press, a member of the Perseus Books Group, [2016]. ISBN: 0813350190; 9780813350196.

[11] Tung-Mow Yan and Sidney D. Drell. "The Parton Model and its Applications". In: *Int. J. Mod. Phys.* A29 (2014), p. 0071. DOI: 10.1142/S0217751X14300713. arXiv: 1409.0051 [hep-ph].

[12] Andy Buckley et al. "LHAPDF6: parton density access in the LHC precision era". In: *Eur. Phys. J.* C75 (2015), p. 132. DOI: 10.1140/epjc/s10052-015-3318-8. arXiv: 1412.7420 [hep-ph].

[13] John C. Collins, Davison E. Soper, and George F. Sterman. "Factorization of Hard Processes in QCD". In: *Adv. Ser. Direct. High Energy Phys.* 5 (1989), pp. 1–91. DOI: 10.1142/9789814503266_0001. arXiv: hep-ph/0409313 [hep-ph].

[14] Wolfram Research Inc. *Mathematica, Version 12.0*. Champaign, IL, 2019.

[15] Adam Alloul et al. "FeynRules 2.0 - A complete toolbox for tree-level phenomenology". In: *Comput. Phys. Commun.* 185 (2014), pp. 2250–2300. DOI: 10.1016/j.cpc.2014.04.012. arXiv: 1310.1921 [hep-ph].

[16] Valentin Hirschi et al. "Automation of one-loop QCD corrections". In: *JHEP* 05 (2011), p. 044. DOI: 10.1007/JHEP05(2011)044. arXiv: 1103.0621 [hep-ph].

[17] Fabio Maltoni and Tim Stelzer. "MadEvent: Automatic event generation with MadGraph". In: *JHEP* 02 (2003), p. 027. DOI: 10.1088/1126-6708/2003/02/027. arXiv: hep-ph/0208156 [hep-ph].

[18] Johan Alwall et al. "New Developments in MadGraph/MadEvent". In: *AIP Conf. Proc.* 1078.1 (2009), pp. 84–89. DOI: 10.1063/1.3052056. arXiv: 0809.2410 [hep-ph].

[19] Pierre Artoisenet et al. "Automatic spin-entangled decays of heavy resonances in Monte Carlo simulations". In: *JHEP* 03 (2013), p. 015. DOI: 10.1007/JHEP03(2013)015. arXiv: 1212.3460 [hep-ph].

[20] Priscila de Aquino et al. *The Higgs Characterisation model*. URL: https://feynrules.irmp.ucl.ac.be/wiki/HiggsCharacterisation.

[21] Matteo Cacciari, Gavin P. Salam, and Gregory Soyez. "FastJet User Manual". In: *Eur. Phys. J.* C72 (2012), p. 1896. DOI: 10.1140/epjc/s10052-012-1896-2. arXiv: 1111.6097 [hep-ph].

[22] Rene Brun and Fons Rademakers. "ROOT - An Object Oriented Data Analysis Framework". In: *Nucl. Inst. and Meth. in Phys. Res. A 389 (1997) 81-86* (). URL: http://root.cern.ch/.

[23] D. de Florian et al. "Handbook of LHC Higgs Cross Sections: 4. Deciphering the Nature of the Higgs Sector". In: (2016). DOI: 10.23731/CYRM-2017-002. arXiv: 1610.07922 [hep-ph].

[24] Morad Aaboud et al. "Measurement of VH, $H \to b\bar{b}$ production as a function of the vector-boson transverse momentum in 13 TeV pp collisions with the ATLAS detector". In: *JHEP* 05 (2019), p. 141. DOI: 10.1007/JHEP05(2019)141. arXiv: 1903.04618 [hep-ex].